

## Chapter 6

# Exciton Energy Transfer in Carbon Nanotubes Probed by Photoluminescence

**Ping Heng Tan,<sup>a,b</sup> Tawfique Hasan,<sup>b</sup> Francesco Bonaccorso,<sup>b</sup>  
and Andrea C. Ferrari<sup>b</sup>**

<sup>a</sup>*State Key Laboratory for Superlattices and Microstructures,  
Institute of Semiconductors, Beijing 100083, China*

<sup>b</sup>*Department of Engineering, University of Cambridge, Cambridge CB3 0FA, UK  
phtan@semi.ac.cn, acf26@hermes.cam.ac.uk*

## 6.1 Introduction

Photoluminescence (PL) spectroscopy is a common technique used for the characterization of semiconductors. The detection of PL from isolated semiconducting single-walled nanotubes (s-SWNTs)<sup>1</sup> has made the optical properties of SWNTs a subject of intense interest.<sup>2-16</sup> Debundling of SWNTs was believed to be an essential prerequisite to observe PL emissions from s-SWNTs. However, Refs. 12 and 17 observed optical signatures from SWNT bundles in aqueous solutions and assigned them to Förster resonance energy transfer (FRET).<sup>12,17</sup>

The exciton binding energies of s-SWNTs are very large, from tens of meVs to 1 eV, depending on diameter, chirality, and dielectric

---

*Luminescence: The Instrumental Key to the Future of Nanotechnology*

Edited by Adam M. Gilmore

Copyright © 2014 Pan Stanford Publishing Pte. Ltd.

ISBN 978-981-4241-95-3 (Hardcover), 978-981-4267-72-4 (eBook)

[www.panstanford.com](http://www.panstanford.com)

screening.<sup>3,4,18</sup> Photoexcited electrons and holes in s-SWNTs can create a bound state of an electron and a hole via Coulomb interaction to form excitons. Excitons dominate the optical properties of SWNTs, even at room temperature, because of their large binding energy.<sup>3,4</sup>

Many works focused on dispersed SWNTs, assuming that sedimentation-based ultracentrifugation (SUF) would completely remove bundles.<sup>1,2</sup> However, small bundles with about 3–10 tubes still exist in most surfactant-assisted SWNT dispersions, even after SUF.<sup>4,12</sup> The formation of bundles in nanotube samples modifies their excitonic behavior, revealed by a change of their optical properties.<sup>19–22</sup> To study the intrinsic optical and electronic properties, completely isolated nanotubes must be used. On the other hand, bundles are necessary in SWNT-based devices, such as saturable absorbers in passively mode-locked lasers and noise suppression filters.<sup>23–34</sup> However, in such applications, the bundle size must be smaller than the device operation wavelength to avoid nonsaturable losses due to scattering.<sup>35</sup>

Thus, quantification of bundling in aqueous dispersions is a key requirement for basic research and applications.

In this chapter, we discuss the spectral features of exciton energy transfer (EET)-induced PL emission from acceptor s-SWNTs in bundles after the resonance excitation of donor s-SWNTs. Moreover, we explain how to distinguish such features from other spectral features in the PL and photoluminescence excitation (PLE) spectra. Then, we discuss the transfer efficiency of excitons and exciton relaxation pathways in bundles. Finally, we discuss how FRET may be utilized for nanotube-based photonic devices.

## 6.2 The Photoluminescence Spectrum of Nanotube Bundles

To confirm the presence of bundles and to study their optical properties, we compare as-prepared SWNT dispersions in D<sub>2</sub>O with sodium dodecylbenzene sulfonate (SDBS) as a surfactant and the same sample after two months (Fig. 6.1a,b). The (6,5) and (7,5) emission peaks observed in Ref. 2 are indicated with two dash-dotted lines. These show a ~1–5 nm blue shift compared to our measurements but on samples prepared with sodium dodecyl sulfate (SDS) as a surfactant.

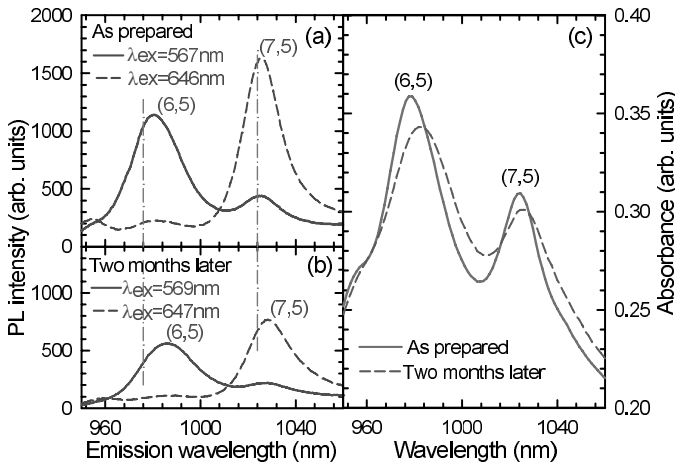


**Figure 6.1** PL emission spectra of (6,5) and (7,5) for (a) an as-prepared dispersion and (b) after two months. (c) Absorption spectra of (6,5) and (7,5) for an as-prepared dispersion and after two months. The dash-dotted lines indicate the PL-peak positions observed in Ref. 2.

Since it was shown that dispersions prepared with similar methods using SDS and SDBS do not have any spectral shift<sup>36</sup>, the effect of dielectric screening on individual SWNTs wrapped by SDS and SDBS is nearly identical in the 850–1,100 nm emission range. We thus assign the red shift in our dispersions compared to Ref. 2 to bundling. The emission peaks of (6,5) and (7,5) from the same dispersion after two months (Fig. 6.1b) red shift by ~3–5 nm relative to the as-prepared dispersion, Fig. 6.1a. This suggests that the bundle size further increases after two months.

The corresponding absorption spectrum in Fig. 6.1c further confirms this, since the absorption peaks are red-shifted and broadened.

Figure 6.2 is a contour plot (known as a “PLE map”), showing the PL emission of the dispersion as-prepared and after two months, as a function of emission and excitation wavelength. The main features in the map are the exciton-exciton resonances. Each resonance spot can be labeled as  $(\lambda_{\text{ex}}, \lambda_{\text{em}})$ , where  $\lambda_{\text{ex}}$  and  $\lambda_{\text{em}}$  are the excitation and emission wavelengths.  $\lambda_{\text{ex}}$  corresponds to the energy of the excitonic states  $eh_{ii}$  associated with the  $i^{\text{th}}$  electronic interband transitions  $E_{ii}$  ( $i = 1, 2, 3, 4$ ) in the single-particle picture, while  $\lambda_{\text{em}}$  represents the

emission energy of the lowest optical-active excitonic transition  $eh_{11}$ . All the observed resonances are indicated with crosses. Some spots, observed in previous results<sup>2</sup> but not in this work, are marked with  $\times$ . The  $(n,m)$  assignments for all resonances are shown in Fig. 6.2.

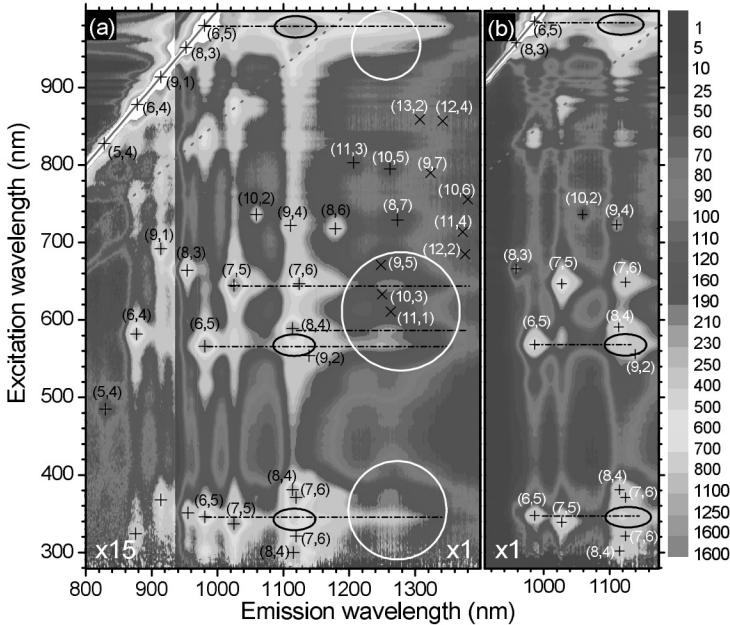


**Figure 6.2** PLE map for (a) an as-prepared dispersion and (b) after two months. Crosses represent  $eh_{11}$  emission of SWNTs for excitation matching their  $eh_{11}$ ,  $eh_{22}$ ,  $eh_{33}$ , and  $eh_{44}$ . Resonances related to  $(eh_{22}, eh_{11})$  observed in Ref. 2 are indicated as  $\times$ . Each resonance is labeled with the chiral index of the corresponding SWNT. The solid lines in the upper-left corners represent resonances with same excitation and recombination energies. The dotted lines are phonon sidebands. Open ellipses mark emission from  $(8,4)$ ,  $(7,6)$ , and  $(9,4)$  with excitation matching the  $(6,5)$   $eh_{11}$ ,  $eh_{22}$ , and  $eh_{33}$ . Open circles mark emission in the 1,200–1,350 nm range, with excitation matching  $eh_{11}$ ,  $eh_{22}$ , and  $eh_{33}$  of  $(6,5)$ ,  $(7,5)$ , and  $(8,4)$ .

In addition to the well-known exciton-exciton resonances, Fig. 6.2a,b shows new features indicated by open ellipses and circles. The exciton-exciton resonances decrease in intensity after two months, again suggesting SWNTs aggregate with time. However, the relative intensity of the (980 nm, 1,118 nm) band becomes

stronger after two months. The two peaks near (568 nm, 1,118 nm), (346 nm, 1,118 nm) (open ellipses, Fig. 6.2b) are better resolved due to the lower intensity of the (8,4), (7,6), and (9,2) exciton-exciton resonances compared to the pristine dispersion. In the 1,200–1,350 nm emission range, exciton-exciton resonances of SWNTs such as (13,2), (12,4), (10,5), (9,7), (10,6), (8,7), (11,4), (12,2), (9,5), (10,3), and (11,1), indicated by crosses and  $\times$ , have weak emission intensities due to their lower concentration in CoMoCAT samples.<sup>65</sup> However, the new features marked by open circles show much stronger intensity than the above exciton-exciton resonances. The excitation energies of all the new features marked by open circles match  $eh_{11}$ ,  $eh_{22}$ , or  $eh_{33}$  of (6,5), (7,5), and (8,4), as indicated by horizontal dash-dotted lines in Fig. 6.2a,b. These features are induced by the resonant excitation of nanotubes with a large bandgap, causing emission from smaller-bandgap SWNTs. This implies EET between SWNTs in bundles, where the larger-gap tubes act as exciton donors (D) and the smaller-gap tubes act as exciton acceptors (A). The EET features can be denoted as  $(eh^D, eh^A)$ , with  $i = 1, 2, 3, \dots$ .

The exciton-phonon interaction is very strong in nanotubes.<sup>37</sup> This can mix an exciton with phonons and form a sideband above the main absorption peak due to strong exciton-phonon coupling.<sup>37</sup> Such sidebands of  $eh_{ii}$  excitons ( $i = 1, 2, \dots$ ) have been resolved in PLE maps of SWNT dispersions<sup>8,9,12</sup>  $\sim 0.215$  eV above the  $eh_{ii}$  excitons. We denote such sidebands as  $eh_{11} + K$  (dotted lines in Fig. 6.2).

Due to the strong exciton-phonon coupling, the main excitonic absorption peak transfers part of its spectral weight to the phonon sideband.<sup>37</sup> Phonon sidebands could be involved in the energy transfer process between adjacent tubes in bundles. However, the observed sideband feature is much weaker than corresponding exciton-exciton resonances.<sup>8,9,12</sup> Thus, the associated EET-features from sidebands should be much weaker and overshadowed by strong exciton-exciton resonances of other nanotube species. Ideally, to unambiguously identify and appropriately assign the weak features related to energy transfer from excitonic phonon sidebands, dispersions enriched with few chiralities and small bundles are required. For this purpose, we enrich SWNTs in a sodium cholate (SC) dispersion via density gradient ultracentrifugation (DGU).<sup>38,39</sup> In DGU, aqueous dispersions of surfactant-encapsulated tubes are ultracentrifuged in a preformed density gradient medium (DGM).

During the process, they move along an ultracentrifuge tube, dragged by the centrifugal force, until they reach the point where their buoyant density equals that of the surrounding DGM, that is, their isopycnic point.<sup>38,39</sup> After DGU, using an upward displacement fraction technique, we extract small aliquots of sorted SWNTs layer by layer.<sup>38,39</sup> In particular we focus on one of the middle fractions. Spectroscopic characterization shows that this dispersion is enriched with small-diameter tubes such as (6,5), (9,1), and (6,4).<sup>39</sup> These tubes are detected in the PLE contour plot, as shown in Fig. 6.3. The PL peaks of the (6,5)  $eh_{11}$  excitonic transitions are  $\sim 7$  nm red-shifted with respect to the topmost fraction of a DGU-enriched sample in Refs. 38 and 39. This indicates the presence of bundles in our dispersion. A further evidence of bundling is the EET-induced ( $eh_{22}^D$ ,  $eh_{11}^A$ ) features from (6,5) to (7,5) and (8,4), indicated by the horizontal solid line in Fig. 6.3.

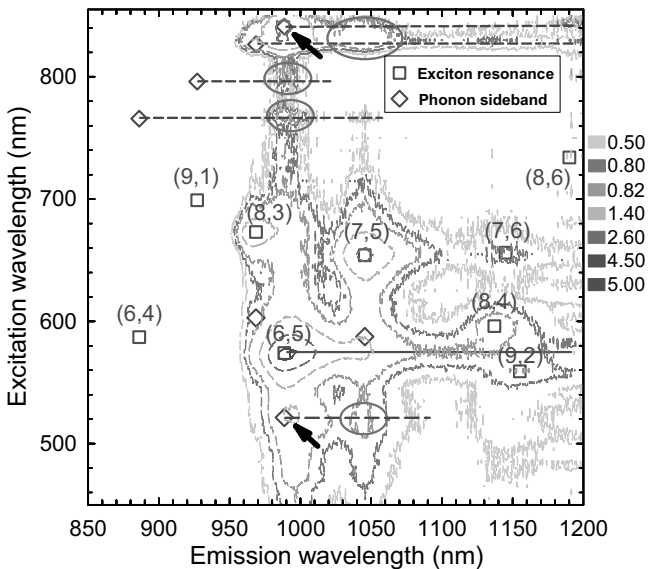


**Figure 6.3** PLE contour plot for the middle fraction of an SC-encapsulated dispersion. Open squares are ( $eh_{22}$ ,  $eh_{11}$ ) exciton resonances, each labeled with the corresponding SWNT chiral index. Open diamonds indicate phonon sidebands for each nanotube species. Arrows indicate phonon sidebands for the (6,5)  $eh_{11}$  and  $eh_{22}$  excitons. Open ellipses show EET-induced features from the resonant excitation of phonon sidebands of SWNTs.

The features marked by open diamonds in Fig. 6.3 are related to the phonon sidebands, whose excitation energy is  $\sim 0.215$  eV higher than the  $eh_{11}$  and  $eh_{22}$  energies. Moreover, the PLE map in Fig. 6.3 shows some intense features marked with open ellipses. Their excitation energy corresponds to the phonon sidebands of (6,5), (6,4), (9,1), and (8,3), as indicated by the dashed lines. Therefore, we attribute these features to PL emission from a smaller-gap nanotube induced by the resonant excitation of phonon sidebands  $eh_{11} + K$ , or  $eh_{22} + K$  of a larger-gap one. For example, the feature at (521 nm, 1,045 nm) corresponds to the resonant excitation of the (6,5)  $eh_{22} + K$  and emission from the (7,5)  $eh_{11}$ . This is a new type of EET feature, resulting from resonant excitation of  $eh_{ii} + K$  ( $i = 1, 2, 3, \dots$ ) phonon sidebands of large-gap SWNTs. The EET-induced features from  $eh_{ii}$  ( $i = 1, 2, 3, \dots$ ) excitons and  $eh_{ii} + K$  ( $i = 1, 2, 3, \dots$ ) sidebands are very common in the PLE maps of nanotube dispersions. For example, Figs. 1b and 5b in Ref. 40 reported a PL peak below  $eh_{11}$  for (6,5) and (7,5) when the excitation matched the corresponding  $eh_{22}$ . McDonald et al.<sup>40</sup> assigned such features to “mid gap emission” (see Figs. 1b and 5b of Ref. 40). We note that this so-called “midgap emission” at (570 nm, 1,130 nm) in Fig. 5b of Ref. 40 matches the (7,6) and (9,4) emission wavelength. We thus assign this feature not to midgap emission but to EET from (6,5) to (7,6) and (9,4). The PL emission associated with EET was also observed in pairs of semiconducting s-SWNTs by high-resolution optical microscopy and spectroscopy<sup>41</sup>, as well as in pairs of suspended SWNTs<sup>42</sup>, and in other nanotube dispersions, freestanding bundles, or double-wall nanotubes.<sup>43-55</sup>

We find that the existence and/or the gradual formation of bundles is inevitable even after debundling procedures.<sup>12</sup> The presence of bundles can be probed by monitoring the EET features in PL and PLE. Figure 6.4 shows the PL and PLE spectra of as-prepared dispersions<sup>12</sup> in SDBS/D<sub>2</sub>O and after two months. The PL spectra are collected resonantly exciting the (6,5)  $eh_{22}$  at  $\sim 568$  nm. (9,4), (8,4), (7,6), (9,2) and (8,6) are nonresonant at this excitation wavelength. Thus, the PL intensity from (9,4), (8,4), (7,6), (9,2), and (8,6) is expected to be very weak compared to that of (6,5). We note that their intensity is comparable to that of (6,5), especially after two months. We also consider that (6,5) have larger PL cross sections<sup>19</sup> and have a higher concentration in the dispersion, as revealed in the absorption spectra (dotted line in Fig. 6.4a) with respect to other tubes. The strong PL emission in the 1,080–1,200 nm range

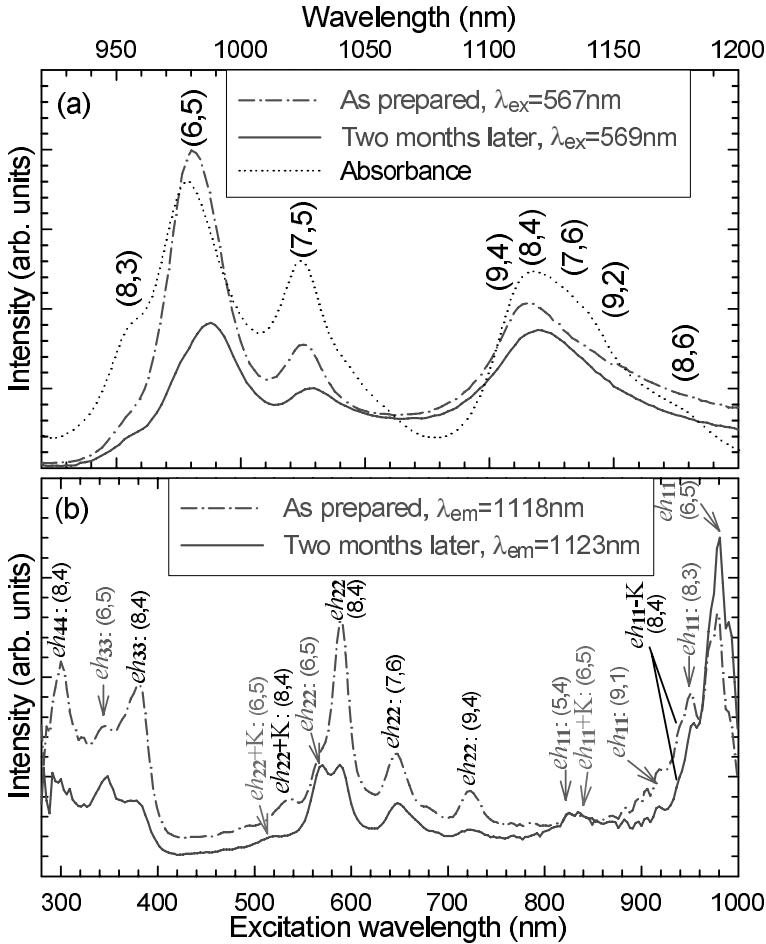


**Figure 6.4** (a) PL (dash-dotted line) and absorption (dotted) spectra of an as-prepared dispersion in  $D_2O/SDBS$  and PL (solid line) of the same dispersion after two months. (b) PLE spectra of an as-prepared dispersion (dash-dotted line) and after two months (solid line). The PLE and PLE wavelengths are indicated.

is attributed to EET from (6,5)  $eh_{22}$  to  $eh_{11}$  of (9,4), (8,4), (7,6), (9,2), and (8,6). In the PLE map, each vertical line provides a corresponding PLE spectrum, revealing high-lying excitonic transitions of specific tubes at its emission wavelength. For the PLE spectra in Fig. 6.4b, we

set the emission wavelength close to  $eh_{11}$  of (8,4), (7,6), and (9,4). The absorption peaks of the (8,4)  $eh_{44}$ ,  $eh_{33}$ , and  $eh_{22}$  excitons, and  $eh_{22} + K$  and  $eh_{11} + K$  phonon sidebands, and of (7,6) and (9,4)  $eh_{22}$  can be identified for the as-prepared dispersion, as indicated in Fig. 6.4b. After two months, the PL intensity of these peaks decreases more than 50%. However, some absorption features are better resolved with respect to the pristine dispersion. After checking the  $eh_{ii}$  ( $i = 1, 2, 3$ ) energy of (6,5), (5,4), (9,1), and (8,3), the EET from the (6,5)  $eh_{ii}$  ( $i = 1, 2, 3$ ) and (5,4), (9,1), and (8,3)  $eh_{11}$  to the (8,4), (7,6), and (9,4)  $eh_{11}$  can be identified.

The broad features at (514 nm, 838 nm) cannot be assigned to any  $eh_{ii}$ ; however, their energy matches the (6,5)  $eh_{22} + K$  and  $eh_{11} + K$  phonon sidebands. Thus, such features are induced by EET from (6,5)  $eh_{22} + K$  and  $eh_{11} + K$  phonon sidebands to (8,4), (7,6), and (9,4)  $eh_{ii}$ . All these EET features are labeled in Fig. 6.4b by arrows.

Thus, in the presence of bundles, the spectra can be explained by EET between donor and acceptor tubes. EET occurs at the  $eh_{11}$  of acceptors when the donor  $eh_{ii}$  ( $i = 1, 2, 3, 4$ ) excitons or  $eh_{ii} + K$  ( $i = 1, 2, 3, 4$ ) phonon sidebands are resonantly excited.

### 6.3 Mechanism and Efficiency of EET in Nanotube Bundles

In low-dimensional systems, exciton tunneling, photon exchange, and FRET are efficient EET mechanisms.<sup>56–61</sup> FRET occurs between a donor (D) molecule in the excited state and an acceptor (A) molecule in the ground state.<sup>56</sup> The donor molecules typically emit at shorter wavelengths that overlap with the absorption spectrum of the acceptor. FRET is a very efficient EET mechanism via resonant, near-field, dipole–dipole interactions.<sup>56</sup> It is commonly observed in biological systems, conjugated polymers, wires, and dots<sup>56,58–61</sup>, where it dominates at short and intermediate distances (0.5–10 nm). Its efficiency is determined by the spectral overlap of donor emission and acceptor absorption, by the donor–acceptor distance, ( $R_{DA}$ ), and by the relative orientation of emission and absorption dipoles.

The transfer rate is proportional to  $R_0^{DA}$ .<sup>56</sup> The FRET efficiency in bundles is expected to be high.<sup>12</sup> Indeed, the emission-absorption overlap between large- and small-gap tubes depends on the specific

donor–acceptor couple. However, excitons can be cascadedly transferred from donor to acceptor, even when a small emission-absorption overlap is present, via intermediate gap tubes within a bundle. Moreover, phonon-assisted absorption<sup>5</sup> of the acceptor nanotube is likely to increase spectral overlap. SWNTs form bundles by aligning themselves parallel too each other, giving a maximum dipole orientation factor. Nanotubes in bundles also have a small wall-to-wall distance. This makes higher multipolar contributions possible.<sup>56,58</sup>

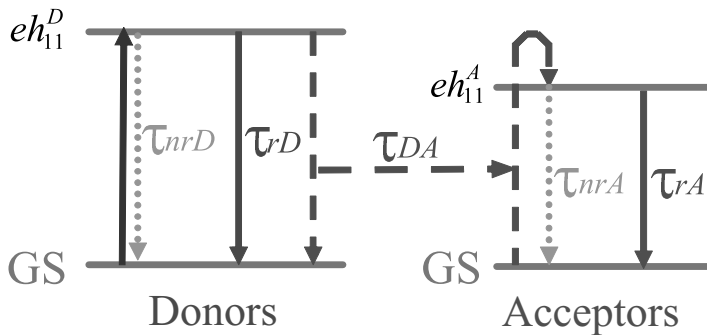


**Figure 6.5** Scheme of exciton relaxation of two nanotubes in a bundle after resonant excitation of the donor  $eh_{11}$ . GS labels the ground states of the donor and the acceptor. In addition to radiative (r) and nonradiative (nr) relaxation of excitons, labeled  $\tau_D$  and  $\tau_{rD}$  for the donor and  $\tau_A$  and  $\tau_{rA}$  for the acceptor, EET with the rate  $\tau_{DA}$  offers another pathway for de-excitation of the donor tube and excitation of the acceptor.

To estimate the energy transfer lifetime between donor and acceptor from experimental results, one can consider the exciton relaxation of two adjacent tubes with different gaps, following the resonant  $eh_{11}$  excitation of the larger-gap tube, as sketched in Fig. 6.5. The rate equations of the donor–acceptor system are:

$$\partial n_D / \partial t = G_{pe} - n_D (1/\tau_{nrD} + 1/\tau_{rD}) - n_D / \tau_{DA} \quad (6.1)$$

$$\partial n_A / \partial t = n_D / \tau_{DA} - n_A (1/\tau_{nrA} + 1/\tau_{rA}) \quad (6.2)$$

where  $\tau_{DA}$  is the energy transfer lifetime between the donor and the acceptor,  $n_D$  is the population of excitons in the donor and  $n_A$  in the acceptor,  $\tau_{nrD}$ ,  $\tau_{rD}$ ,  $\tau_{nrA}$ , and  $\tau_{rA}$  are the radiative (r) and nonradiative (nr) lifetimes, and  $G_{pe}$  the exciton density in the donor created by photoexcitation. We get the ratio of acceptor emission intensity ( $I_A =$

$n_A/\tau_{rA}$ ) to the donor ( $I_D = n_D/\tau_{rD}$ ) from Eqs. 6.1 and 6.2 at the steady state,

$$I_A/I_D = \frac{1/\tau_{DA}}{1/\tau_{rA} + 1/\tau_{nrA}} \frac{\tau_{rD}}{\tau_{rA}} \quad (6.3)$$

The  $eh_{11}$  radiative lifetime is  $\sim 20$ – $180$  ps, depending on temperature.<sup>62</sup> For tube diameters  $\approx 0.75$ – $0.95$  nm, it is  $\sim 20$ – $30$  ps at room temperature.<sup>63</sup> This is much shorter than the theoretical radiative lifetime ( $\sim 10$  ns).<sup>64</sup> Thus, the observed lifetimes are determined by nonradiative recombinations. Eq. 6.3 can be simplified as,

$$I_A/I_D \approx \tau_{nrA}/\tau_{DA} \cdot \quad (6.4)$$

We measured a very high  $I_A/I_D$  in bundles.<sup>12</sup> For example, under (5,4) and (6,5)  $eh_{11}$  excitation in Fig. 6.2a, the ratio of PL intensity of all acceptor tubes to that of the (5,4) and (6,5) donors is  $\sim 75$  and  $1.0$ , respectively. Some (5,4) and (6,5) tubes could be isolated. Thus, the above intensity ratio represents a lower limit. From Eq. 6.4, the energy transfer lifetime can be estimated as  $\sim 0.3$  ps. This means that exciton relaxation in bundles by EET can be comparable or even faster than nonradiative recombination. This fast relaxation suppresses the PL emission from donors but, on the other hand, significantly increases the acceptors' luminescence.

In principle, the EET efficiency can be defined as the ratio between the excitons generated in the acceptors by EET and all the donor  $eh_{11}$  photoexcited excitons. If we assume  $\tau_{nrA} \approx \tau_{nrD}$ , the EET efficiency,  $\eta_{DA}$ , is given by:

$$\eta_{DA} = \frac{n_D}{\tau_{DA}} / G_{pe} \approx \frac{\tau_{nrA}/\tau_{DA}}{1 + \tau_{nrA}/\tau_{DA}} \approx \frac{I_A/I_D}{1 + I_A/I_D} \quad (6.5)$$

If we neglect the loss of excitons from excited excitonic states to  $eh_{11}$  for the donor nanotubes, the above results can also be used to estimate the efficiency of different EET processes, such as ( $eh^D$ ,  $eh^A$ ) and ( $eh^D + K$ ,  $eh^A$ ).

Considering the energy transfer from the (5,4) and (6,5)  $eh_{11}$  to the  $eh_{11}$  of their acceptors in Fig. 6.2a, and from the  $eh_{22} + K$  of (6,5) donors to the (7,5) acceptors  $eh_{11}$  in Fig. 6.3, we can estimate an efficiency of  $\sim 50$ – $98\%$  for  $eh_{11}$  resonant excitation and  $\sim 33\%$  for  $eh_{22} + K$  resonant excitation. These estimates indicate that the EET efficiency is very high when the  $eh_{ii}$  or phonon sideband of donors

are resonantly excited. Again, because some isolated tubes may exist in the dispersion, these estimates need be considered lower limits.

To quantify the EET efficiency and rate, Förster theory should be considered.<sup>56</sup> The energy transfer efficiency depends on the spectral overlap of emission and absorption bands. In the case of nanotubes in bundles, the donor and acceptor are two parallel tubes with a small wall-to-wall distance; thus the total transfer rate from a locally excited donor can be estimated by integrating the rates along the axis of the acceptor nanotube, as detailed by Qian et al.<sup>41</sup> The experimental results reproduce the low quantum yield ( $10^{-2}$ – $10^{-3}$ ) for PL emission from s-SWNTs.<sup>1</sup>

We also consider two other possible mechanisms for EET: tunneling and photon exchange. Tunneling requires coupling of exciton wave functions.<sup>57</sup> Its rate decays rapidly with  $R_{DA}$  and is very sensitive to the  $eh_{11}$  energy difference. The 16 species detected in our experiment have diameters  $\approx 0.65$ – $1.05$  nm,  $\Delta(eh_{11}) \approx 0.06$ – $0.5$  eV, and chiral angle variation  $\approx 5$ – $26^\circ$ .<sup>65</sup> Therefore, the efficiency should strongly depend on the specific donor–acceptor couple. However, the experimental results show no  $(n,m)$  preference. Therefore, exciton tunneling is not expected to be the dominant EET mechanism.

On the other hand, photon exchange consists in exciton–photon coupling with no direct donor–acceptor interaction. It has a smaller dependence on  $R_{DA}$  than FRET; thus it can become significant for much longer distances than FRET. However, the lack of significant EET features in isolated tubes in solution<sup>2,65</sup>, combined with the low quantum efficiency<sup>1</sup>, suggest that even if photon exchange may weakly contribute to EET between nanotube bundles or between isolated SWNTs, it is not dominant between adjacent tubes in a given bundle.

## 6.4 How to Distinguish EET-Induced Features from Other Sidebands in the PL Spectrum?

In addition to the features associated with exciton–exciton resonances, phonon sidebands, and EET, other sidebands are also observed. In general, a sideband can be classified as an excitation or an emission sideband. The excitation sideband includes phonon-assisted absorptions,  $eh_{ii} + \text{phonons}$ <sup>5,6,42</sup>, and phonon sidebands  $eh_{ii}$

+ K,<sup>8,9,12,14</sup> while the emission sidebands could be due to EET<sup>12,17,41</sup>, K-phonon sidebands  $eh_{ii}$ -K<sup>13-16</sup>, triplet dark excitons<sup>16</sup>, and emission of  $eh_{ii}$ -phonons.<sup>5,13</sup>

For the emission sideband, triplet dark excitons can only be observed in samples after pulsed-laser irradiation.<sup>16</sup> The intensity of phonon-assisted emissions, such as  $eh_{11} - G$ , is very weak.<sup>16</sup> Thus, we focus on how to distinguish the EET and  $eh_{ii}$ -K phonon sidebands. The  $eh_{ii}$ -K phonon sideband was initially interpreted as “deep dark excitonic (DE) states” by Kiowski et al.<sup>13</sup> In these, the energy separation between  $eh_{11}$  and “deep DE states” (Fig. 3 in Ref. 13) depends on the SWNT diameter and varies from ~95 meV for 0.75 nm tubes to ~140 meV for 1.1 nm tubes. However, recently, several groups demonstrated no diameter dependence for this sideband.<sup>14-16</sup> The explanation of the energy separation between the  $eh_{11}$  and  $eh_{ii}$ -K sideband for small-diameter tubes is a key issue to clarify the above contradictory results. One possible explanation is that the so-called “DE states” observed by Kiowski et al.<sup>13</sup> may be derived from triplet dark excitons. This assumption can be excluded by comparing the observed “DE states” (solid circles) and triplet dark excitons (solid diamonds), as shown in Fig. 6.7. In fact, considering the donor/acceptor pairs (6,5)/(10,2), (9,1)/(8,7), (7,5)/(8,4), and (10,2)/(8,6), the energy separation between the  $eh_{11}$  of those donor/acceptor pairs is in good agreement with the energy difference between  $eh_{11}$  and the so-called “DE states” for the corresponding donor tubes, as shown in Fig. 6.3 of Kiowski et al.<sup>13</sup> Therefore, the “DE states” features reported by Kiowski et al.<sup>13</sup> for small-diameter tubes, such as (6,5), (9,1), (7,5), and (10,2), can be in fact assigned as EET sidebands of donor/acceptor pairs, such as (6,5)/(10,2), (9,1)/(8,7), (7,5)/(8,4), and (10,2)/(8,6).

To distinguish between EET and  $eh_{ii}$ -K phonon sidebands, we compare the PLE maps of a dispersion in SDBS and the top fraction of a sorted dispersion in SC by DGU<sup>39</sup>, as shown in Fig. 6.6. The former is enriched with bundles, while the latter is highly enriched in isolated tubes, where ~90% of s-SWNTs are (6,5).<sup>39</sup> As shown in Fig. 6.6a,b, for dispersions in SDBS containing bundles, the EET features can be very strong due to the bundling of (6,5) and (8,4), forming donor-acceptor pairs. In Fig. 6.6c, because of the removal of (8,4) acceptors in the topmost fraction, and the high enrichment of isolated (6,5), the EET from (6,5) to (8,4) is not seen. Instead, only the (6,5)  $eh_{11}$ -K sidebands can be seen, down-shifted ~21 meV from

the EET from (6,5) to (8,4). Figure 6.6c shows that the PL intensity of the  $eh_{ii}$ -K sidebands for the top fraction is only  $\sim 7\%$  of the main  $eh_{11}$  peaks, which have a much smaller intensity than EET features. EET is a major relaxation channel for exciton decay in bundles, which can quench the PL emission from donors. It is expected for the  $eh_{ii}$ -K sidebands to be weaker in bundles than in isolated tubes. Therefore, in the dispersions containing bundles, the  $eh_{ii}$ -K sidebands may be too weak to be clearly observed if they are partially shadowed by the tails of strong EET features, as shown in Fig. 6.6a,b.

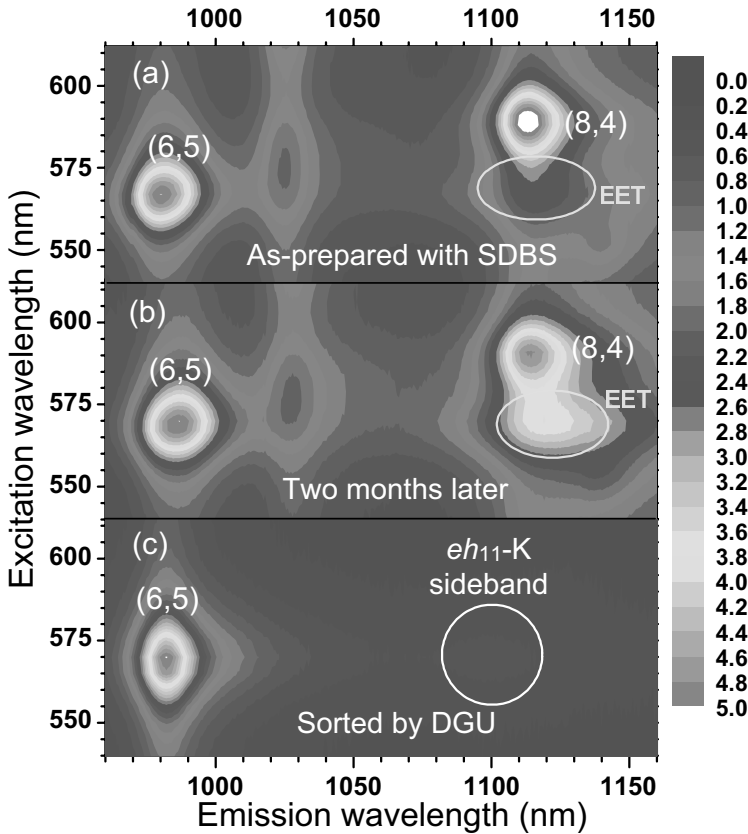


**Figure 6.6** PLE maps of (a) an as-prepared dispersion in SDBS and (b) after two months. (c) PLE map of an as-prepared DGU dispersion in SC. All the maps are normalized by the intensity of (6,5) ( $eh_{22}, eh_{11}$ ) resonances. The ellipses show the EET-induced features, and the circle indicates the (6,5)  $eh_{11}$ -K emission sideband.

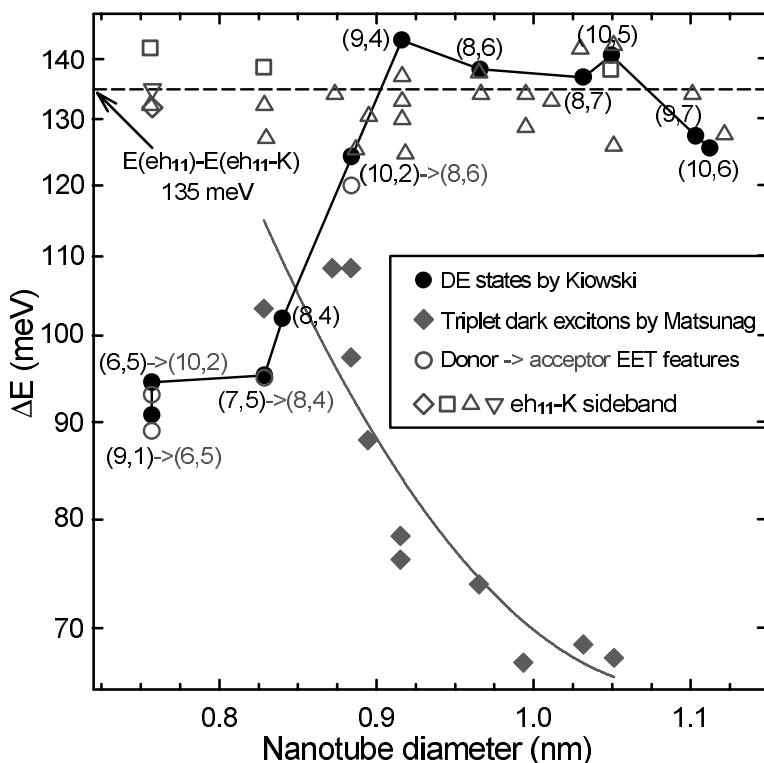


**Figure 6.7** Energy separation ( $E$ ) between  $eh_{11}$  and its lower energy sideband as a function of tube diameter: so-called DE states<sup>13</sup>, EET features<sup>12</sup>, triplet dark excitons<sup>16</sup>, and  $eh_{11}$ -K sidebands ( $\diamond$ ,<sup>14,15,6</sup> and  $\nabla$  in Fig. 6.6). The typical value ( $\sim 135$  meV) of energy separation between  $eh_{11}$  and  $eh_{11}$ -K phonon sideband is indicated.

Table 6.1 compares EET and  $eh_{11}$ -K sidebands. The  $eh_{11}$ -K sidebands can be observed in isolated nanotube dispersions if they are not shadowed by the intense exciton–exciton resonances of other nanotube species. The intensity and peak position of  $eh_{11}$ -K satellites of a given nanotube species are only determined by the main  $eh_{11}$  PL emission peaks of this nanotube. But, the EET peak position depends on both donors and acceptors, with donors determining the excitation position and acceptors the emission. The EET intensity is dominated by the bundling of donors and acceptors. EET features can be comparable to, even much stronger, than the PL emission of the corresponding donors or acceptors. Therefore, it is

easy to distinguish the EET features from  $eh_{11}$ -K satellites in the PLE maps of a dispersion.

**Table 6.1** Comparison between EET features and  $eh_{11}$ -K sidebands in PLE maps of nanotube dispersions

	EET	$eh_{ii}$ -K
Satellites	emission bundles	emission isolated or bundles
Dispersions	strong, dependent	weak, dependent on the main
Intensity	on D-A pairs	peak fixed, $\sim 135$ meV below
Position	dependent on D-A pairs	$eh_{11}$ -K

## 6.5 Relaxation Pathways of Excitons in Nanotube Bundles

The dynamics of creation, relaxation, nonradiative decay, and radiative recombination of excitons and corresponding sidebands is a fundamental issue in nanotube research. The relaxation of excitons in bundles includes two parts. The first is the exciton relaxation in an individual tube (donor or acceptor). The second is the exciton relaxation between donor and acceptor tubes via EET. The total decay rate of an individual tube is  $\tau r + \tau nr \approx 20\text{ps}^{-1}$  at room temperature, dominated by  $\tau_{nr}$ .<sup>62,63,66</sup> The intersubband exciton relaxation from  $eh_{22}$  to  $eh_{11}$  transitions is within  $\sim 150$  fs, with a time constant  $\approx 40$  fs.<sup>67</sup> The maximum EET rate  $\tau_{DA}$  is  $\sim 0.3\text{ps}^{-1}$ , as estimated by Eq. 6.4. Therefore, the donor tubes transfer their exciton energy to acceptors via the lowest optical excitonic states of the donor tubes.

Figure 6.8 shows PLE spectra of isolated (6,5)  $eh_{11}$  and  $eh_{11}$ -K in the top fraction of an SC-encapsulated SWNT dispersion sorted by DGU, in an excitation range of  $eh_{22} + K$  to  $eh_{11} + K$ . The corresponding PLE map is shown in Fig. 6.6c. The excitonic transitions of  $eh_{22} + K$ ,  $eh_{22}$ , and  $eh_{11} + K$  are identified. Additionally, there exists an EET-induced feature from the (8,3)  $eh_{11} + K$  phonon sideband to the (6,5)  $eh_{11}$  sideband. Multiplied by 13, the PL intensity of the  $eh_{11}$ -K sideband becomes similar to that of  $eh_{11}$  over the entire excitation range. This suggests that for PL emission at the  $eh_{11} + K$  sideband, the high-lying excitonic states, such as  $eh_{22} + K$ ,  $eh_{22}$ , and  $eh_{11} + K$ , do not directly relax down to  $eh_{11}$ -K states but relax to  $eh_{11}$  states. Part

recombine at  $eh_{11}$ ; others relax to  $eh_{11}$ -K states and recombine there. Relaxation pathways down to  $eh_{11}$  and  $eh_{11}$ -K directly from specific high-lying excitonic states would result in a different intensity ratio of  $eh_{11}$ -K to  $eh_{11}$ .

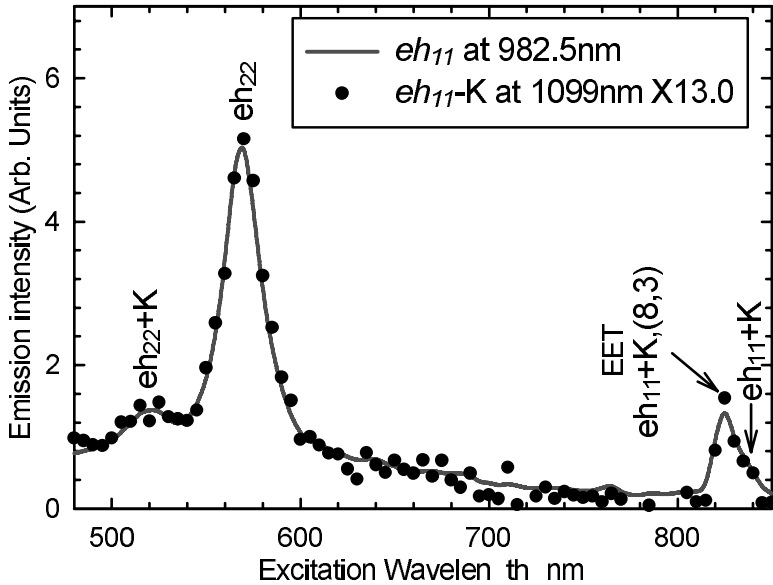


**Figure 6.8** PLE spectra of  $eh_{11}$  and  $eh_{11}$ -K of isolated (6,5) tubes in the top fraction of an SC-encapsulated SWNT dispersion sorted by DGU. The detection wavelength is 982.5 nm for  $eh_{11}$  and 1,099 nm for  $eh_{11}$ -K. The PL intensity of  $eh_{11}$ -K is multiplied by a factor 13. The EET features from  $eh_{11} + K$  phonon sidebands of (8,3) to (6,5)  $eh_{11}$  are also identified.

The relaxation pathways of photoexcited excitons in bundles are illustrated in Fig. 6.9 in the case of the resonant excitation of  $eh_{22}$  and  $eh_{11}$  and/or their phonon sidebands. The weak relaxation pathway associated with phonon-assisted absorption and emission is not considered here. The EET recombination mechanism is as follows: photons are resonantly absorbed by the high-lying excitonic and exciton-phonon bound states of donors; the photoexcited excitons first quickly relax to the  $eh_{11}^D$  states; then some radiatively recombine at the  $eh^D$  of the donor nanotubes, or further relax down to  $eh_{11}^D$ -K and recombine there, while others resonantly transfer their energy to the excitons of acceptors.<sup>12</sup> Finally, the latter radiatively

recombine at the corresponding  $eh_{11}^A$  or further relax down to  $eh_{11}^A - K$  and recombine.

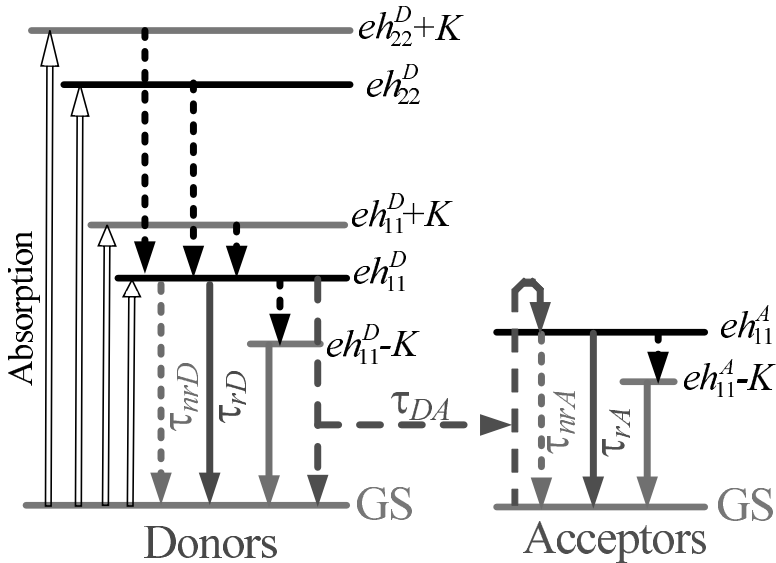


**Figure 6.9** Schematic diagram of exciton absorption (open lines) and relaxation process in a donor–acceptor pair in s-SWNT bundles. Solid lines suggest possible radiative relaxation pathways. Dotted lines indicate possible nonradiative relaxation pathways. Dashed lines represent the EET pathways within a donor–acceptor pair.

## 6.6 How to Detect Bundles and Probe Their Concentration?

The quantification of bundling is important for both fundamental studies and applications. Bundling induces a red shift and broadening of excitonic transitions.<sup>3,12,20</sup> The red shift is attributed to the modification of Coulomb interactions by the dielectric screening induced by other adjacent tubes.<sup>3</sup> Thus, the red shift of the optical transitions in Raman, absorption, and PL spectra can be an indication of bundles.<sup>3,12,20</sup> The optical transitions of SWNTs are strongly modulated by different dielectric environments.<sup>18,22,68–74</sup> Therefore, care must be taken when using the peak shift of optical transitions to identify the presence of bundles, because this may also be induced

by the dielectric environment rather than just bundling. Also, the red shift caused by bundling can be neutralized by the blue shift induced by a change in the dielectric environment. Therefore, detection of bundles through Raman, absorption, and PL measurements requires a reference sample with isolated nanotubes in the same solvent-surfactant environment to quantify the change of optical transitions due to bundling, which is not straightforward for all the pure solvent or solvent-surfactant systems.

The EET spectral features in one-photon PLE maps can be used as fingerprints of bundles. Two-photon excitation spectroscopy was used to estimate the exciton-binding energies in nanotubes.<sup>3,4</sup> Figure 6.10 represents the main features of the two-photon map in Fig. 1 of Ref. 4 and in Fig. 2 of Ref. 3, where HiPco SWNTs were used. This shows several peaks, indicated by solid squares and circles, with a larger excitation energy than the two-photon exciton resonance (open circles). There seems to be a Rydberg-like series of states for every SWNT; however, each of them matches the excitation energy of a larger-gap SWNT, as indicated by each horizontal dashed line in Fig. 6.10. These are analogous to the EET-induced peaks in one-photon excitation spectroscopy in Figs. 6.2 and 6.3. We attribute them to PL emission of small-gap tubes due to EET from larger-gap tubes in bundles. We assign the four features in Fig. 6.10a with  $\sim 1,390$  nm excitation (solid squares) to EET from a (5,4) donor to (6,4), (9,1), (8,3), and (6,5) acceptors, although the concentration of (5,4) is very low in HiPco SWNTs and its two-photon exciton resonance is not observed in Fig. 6.10a. The EET-induced two-photon spectra show more distinct resonance peaks compared to Figs. 6.2 and 6.3. The EET from s-SWNTs to metallic ones is much faster than within s-SWNTs. Thus the PL emission from the latter in one-photon excitation can be heavily quenched due to the presence of m-SWNTs. Therefore, the EET signals should be very weak in the one-photon PLE maps for samples containing a high concentration of m-SWNTs, such as HiPco samples<sup>2</sup>, where m-SWNTs constitute  $\sim 1/3$  of the total. However, interestingly, two-photon excitation of HiPco dispersions<sup>3,4</sup> can exhibit strong EET features, as discussed above. The observation of significant EET features from (5,4) donors reveals that very high EET efficiency can occur in two-photon excitations. It also indicates that the EET rate from s- to m-SWNTs is not so fast to be totally quenched in two-photon excitation. Also, two-photon luminescence increases quadratically with the excitation power. Therefore, in comparison to

one-photon excitation, two-photon excitation spectroscopy can be used as a more sensitive tool to probe bundling.

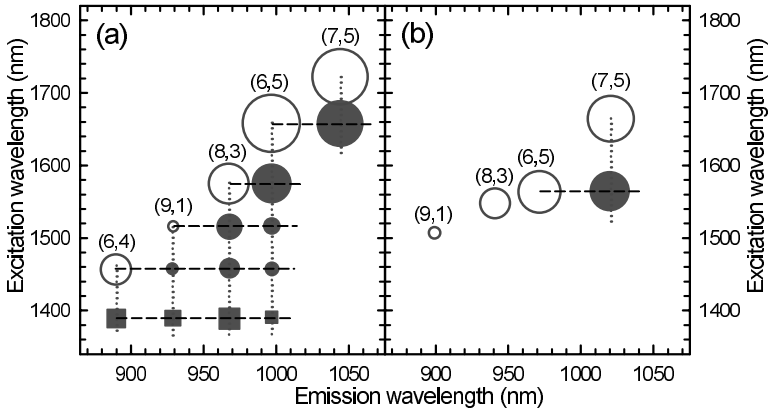


**Figure 6.10** Main features in the two-photon PLE maps reported by (a) Maultzsch et al.<sup>4</sup> and (b) Wang et al.<sup>3</sup>

Open circles are two-photon PLE peaks, each labeled with the corresponding SWNT chiral index. Solid circles and squares are EET peaks.

Because the optical transitions of SWNTs are usually very broad due to bundling inhomogeneity, packing efficiency and dispersion of bundle size, absorption, and PL spectra are not sensitive probes of bundle size in dispersions and in composites. Moreover, if the concentration of some species of nanotubes is low, their PL and absorption features are expected to be shadowed by intense signal from nanotubes with a high concentration. However, the EET intensity can be much stronger than that of exciton–exciton resonances of donor or acceptor nanotubes. The position of EET features can also be far away from exciton–exciton resonances of donor or acceptor tubes. Thus, the EET optical signatures can be used to probe the presence of low-concentration donor or acceptor tubes and to quantify the bundling of a donor–acceptor pair. As shown in Fig. 6.10a, although the (5,4) concentration is very low in HiPco samples<sup>2</sup>, the detection of an EET signal from (5,4) donors indicates their presence. The EET from  $eh_{ii}^D$  and  $eh_{ii}^D + K$  sidebands ( $i = 1, 2, \dots$ ) of donors to  $eh_{11}^A$  excitons of acceptors is an intrinsic optical signature of bundles, independent of the influence of the surrounding dielectric environment.

Therefore, the EET-induced emissions from acceptors in the PL and PLE spectra are a direct, simple, and independent way to identify bundling.

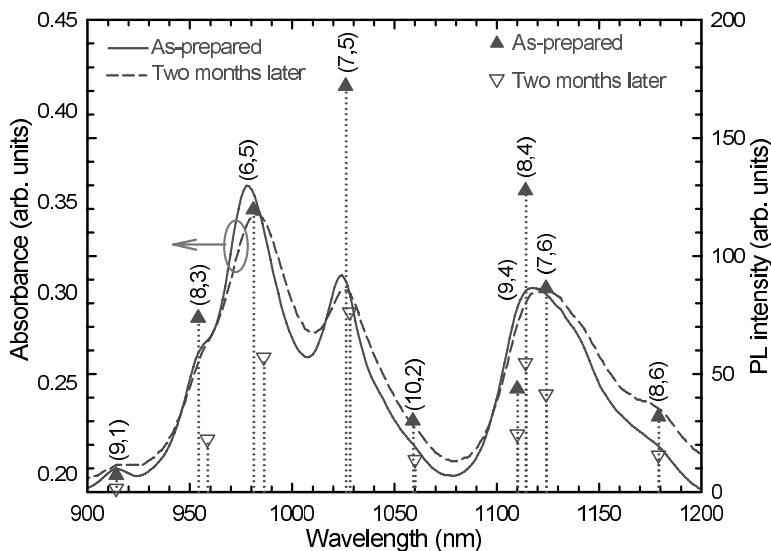


**Figure 6.11** Absorption spectra (solid and dashed lines) and PL intensity of each exciton–exciton resonance (and) of an as-prepared dispersion and after two months.

The PL, PLE, and absorption spectra have been widely used to determine the concentration of nanotubes after correction by the theoretical cross-sections of different chiralities.<sup>75–78</sup> When bundles are present in dispersions or composites, the additional EET relaxation pathway decreases the PL intensity from donors and enhances that from acceptors. The presence of m-SWNTs also strongly quenches the luminescence from s-SWNTs. Figure 6.11 shows the absorption spectra and PL intensity of each exciton–exciton resonance of an as-prepared dispersion in SDBS/D<sub>2</sub>O and after two months. It was reported that the theoretical PL intensity of an individual (6,5) tube is ~20% stronger than for a (7,5).<sup>75</sup> The (6,5) absorption intensity is also much stronger than that of (7,5), as shown in Fig. 6.3a. Thus, the (6,5) PL intensity is expected to be stronger than (7,5) if all nanotubes are individualized. However, Fig. 6.11a shows that in our case (7,5) tubes have much stronger PL emissions. The red shift in the absorption and PL spectra confirms

that the SWNTs in the as-prepared dispersion contain small SWNT bundles. Note that the (6,5) absorption peak width ( $\sim 45$  meV) is  $\sim 31$  meV broader than in (7,5). This implies that the (6,5) dielectric environment and the bundling status (e.g., size distribution of bundles) is more complex than for the (7,5). Compared to isolated tubes<sup>2,65</sup>, additional EET relaxation channels exist in bundles. Therefore, for dispersions where the presence of bundles and their size distribution cannot be conclusively determined, the ( $eh_{22}$ ,  $eh_{11}$ ) intensity of each nanotube species does not necessarily reflect its abundance, contrary to what is sometimes suggested<sup>76,79</sup>, even if the experimental PL is normalized with respect to concentrations and theoretical cross sections.<sup>75</sup> Considering that the absorption spectra of dispersions incubated for two months show a similar profile with respect to the as-prepared dispersions, we conclude that absorption spectroscopy is a more reliable technique to determine the concentration distribution of nanotubes in dispersions.

## 6.7 Exploiting EET for Photonic and Optoelectronic Applications

SWNTs show strong saturable absorption, that is, they become transparent under high-power irradiation.<sup>30,67,80–82</sup> SWNTs are thus suitable for application as mode lockers in ultrafast lasers and noise suppression filters.<sup>23–33</sup> SWNT-based saturable absorbers must be carefully designed to keep a balance between high modulation depth, depending on SWNT concentration, and unwanted nonsaturable losses, due to scattering from large bundles or entanglements, as well as from the polymer matrix, surfactant, residual catalyst particles, and carbon impurities.<sup>30</sup> To ensure fast device operation, the relaxation time of the saturable absorber must be as short as possible. The relaxation time is longer in isolated SWNTs than in bundles.<sup>66,83,84</sup> Hence, bundles are necessary in SWNT-based saturable absorbers, but their size must be smaller than the device operation wavelength to avoid nonsaturable losses due to scattering.<sup>35</sup> EET can thus be used to estimate bundling during the fabrication of such devices.

Dang et al.<sup>53</sup> used EET to monitor the effect of bundling on the efficiency of SWNT-based photovoltaic devices. They reported that bundling of large-gap s-SWNTs with smaller-gap s-SWNTs and

m-SWNTs leads to a 1% reduction in power conversion efficiency in a dye-sensitized solar cell.<sup>53</sup>

Considering the application of bundles as optically pumped light-emitting devices, one must choose a pump laser whose wavelength or photon energy resonantly matches that of the nanotubes to achieve a high excitation efficiency for light emission. One could exploit EET, by matching the pump laser energy with the  $eh_{ii}$  or  $eh_{ii} + K$  of donor nanotubes, to induce an higher emission efficiency from acceptor tubes. This can also extend the wavelength or photon energy of the pump laser for the application of semiconducting bundles as optically pumped light emitters. Since m-SWNTs quench the luminescence from s-SWNTs, small bundles entirely made of s-SWNTs can be ideal for this application.

EET can be also used as a means to concentrate excitons, for example, for photovoltaic applications.<sup>39,48</sup> Han et al.<sup>48</sup> demonstrated a core-shell SWNT filament to concentrate excitons, demonstrating the viability of this concept.<sup>48</sup> Enriched SWNTs were dielectrophoretically spun to fabricate the core-shell filament, with small-gap SWNTs forming the inner or collector core, consisting predominantly of (8,7), (7,6), (11,3), (7,5), and (6,5), and large-gap SWNTs the outer absorbing shell, consisting of (6,5) only. When this filament is irradiated by a broadband light ranging from ultraviolet to near infrared, it exhibits a broadband absorption consistent with the SWNT population in the filament. This also confirms EET can occur between two SWNTs with a small emission-absorption overlap in a cascaded way via intermediate-gap tubes within a bundle.<sup>12</sup> Therefore, the emission of a core-shell nanotube filament is dominated by the smallest-gap tube—(8,7) in the case of Ref. 48—as a result of exciton funneling via EET to the core from the collector, as well as within the core by cascaded EET, from other species to the (8,7).<sup>48</sup> Similar structures consisting of enriched SWNTs can also be used for other devices to achieve an higher absorption bandwidth over a desired window, which could find application in various optoelectronic devices, including photodiodes and bolometers.<sup>48</sup>

## 6.8 Conclusions

We reviewed the use of PL, absorption, and PLE spectroscopy to investigate the optical properties of nanotube bundles. The existence

and gradual formation of bundles in aqueous dispersions is inevitable even after ultrasonication followed by ultracentrifugation. With time, the emission and absorption spectra show weaker intensities and broader spectral profiles. Emission sidebands are observed in the PLE map, assigned to EET between bundled tubes. The EET features correspond to the excitation of donor tubes and the emission of acceptor tubes, and their intensity depends on bundling. The EET intensity can be much stronger than of exciton–exciton resonances of individual donor and acceptor tubes.

EET can be used for 1) nanotube bundle engineering to enhance and improve PL emission from small-bandgap nanotube acceptors for optoelectronics; 2) an additional relaxation channel for excitons, useful for ultrafast photonic devices; 3) investigation of optoelectronic interactions of hybrid structures of SWNTs and other materials, such as quantum dots, conjugated polymers, and biomolecules; 3) explanation of the complex spectral features in the PLE map of nanotube dispersions and composites; 4) provision of a direct, simple, and independent way to identify the presence of bundles or to confirm the presence of only individual isolated nanotubes; and 5) fingerprinting of bundles with different tube concentrations.

## Acknowledgments

We acknowledge funding from the ERC grant NANOPOTS, the EPSRC grant EP/G042357/1, the Royal Society Wolfson Research Merit Award, a Newton International Fellowship, EU grants RODIN and Marie Curie ITN-GENIUS (PITN-GA-2010-264694), the Nokia Research Centre Cambridge, Chinese special fund for Major State Basic Research Project No. G2009CB929301, and NSFC (Nos. 10874177 and 10934007), King's college, Cambridge.

## References

1. M. J. O'Connell, S. M. Bachilo, C. B. Huffman, V. C. Moore, M. S. Strano, E. H. Haroz, K. L. Rialon, P. J. Boul, W. H. Noon, C. Kittrell, J. P. Ma, R. H. Hauge, R. B. Weisman, R. E. Smalley, *Science*, **297**, 593 (2002).
2. S. M. Bachilo, M. S. Strano, C. Kittrell, R. H. Hauge, R. E. Smalley, R. B. Weisman, *Science*, **298**, 2361 (2002).
3. F. Wang, G. Dukovic, L. E. Brus, T. F. Heinz, *Science*, **308**, 838 (2005).

4. J. Maultzsch, R. Pomraenke, S. Reich, E. Chang, D. Prezzi, A. Ruini, E. Molinari, M. S. Strano, C. Thomsen, C. Lienau, *Phys. Rev. B*, **72**, 241402(R) (2005).
5. S. G. Chou, F. Plentz, J. Jiang, R. Saito, D. Nezich, H. B. Ribeiro, A. Jorio, M. A. Pimenta, Ge. G. Samsonidze, A. P. Santos, M. Zheng, G. B. Onoa, E. D. Semke, G. Dresselhaus, M. S. Dresselhaus, *Phys. Rev. Lett.*, **94**, 127402 (2005).
6. H. Htoon, M. J. O'Connell, S. K. Doorn, V. I. Klimov, *Phys. Rev. Lett.*, **94**, 127403 (2005).
7. Y. Z. Ma, L. Valkunas, S. L. Dexheimer, S. M. Bachilo, G. R. Fleming, *Phys. Rev. Lett.*, **94**, 157402 (2005).
8. F. Plentz, H. B. Ribeiro, A. Jorio, M. S. Strano, M. A. Pimenta, *Phys. Rev. Lett.*, **95**, 247401 (2005).
9. Y. Miyauchi, S. Maruyama, *Phys. Rev. B*, **74**, 035415 (2006).
10. Y. Miyauchi, M. Oba, S. Maruyama, *Phys. Rev. B*, **74**, 205440 (2006).
11. J. Lefebvre, P. Finnie, *Phys. Rev. Lett.*, **98**, 167406 (2007).
12. P. H. Tan, A. G. Rozhin, T. Hasan, P. Hu, V. Scardaci, W. I. Milne, A. C. Ferrari, *Phys. Rev. Lett.*, **99**, 137402 (2007).
13. O. Kiowski, K. Arnold, S. Lebedkin, F. Hennrich, M. M. Kappes, *Phys. Rev. Lett.*, **99**, 237402 (2007).
14. O. N. Torrens, M. Zheng, J. M. Kikkawa, *Phys. Rev. Lett.*, **101**, 157401 (2008).
15. Y. Murakami, B. Lu, S. Kazaoui, N. Minami, T. Okubo, S. Maruyama, *Phys. Rev. B*, **79**, 195407 (2009).
16. R. Matsunaga, K. Matsuda, Y. Kanemitsu, *Phys. Rev. B*, **81**, 033401 (2010).
17. P. H. Tan, T. Hasan, F. Bonaccorso, V. Scardaci, A. G. Rozhin, W. I. Milne, A. C. Ferrari, *Phys. E*, **40**, 2352 (2008).
18. V. Perebeinos, J. Tersoff, P. Avouris, *Phys. Rev. Lett.*, **92**, 257402 (2004).
19. S. Reich, C. Thomsen, P. Ordejon, *Phys. Rev. B*, **65**, 155411 (2002).
20. M. J. O'Connell, S. Sivaram, S. K. Doorn, *Phys. Rev. B*, **69**, 235415(2004).
21. F. Wang, M. Y. Sfeir, L. M. Huang, X. M. H. Huang, Y. Wu, J. Kim, J. Hone, S. O'Brien, L. E. Brus, T. F. Heinz, *Phys. Rev. Lett.*, **96**, 167401 (2006).
22. A. G. Walsh, A. N. Vamivakas, Y. Yin, M. S. Ünlü, B. B. Goldberg, A. K. Swan, S. B. Cronin, *Nano Lett.* **7**, 1485 (2007).
23. S. Yamashita, S. Maruyama, Y. Murakami, Y. Inoue, H. Yaguchi, M. Jablonski, S. Y. Set, *Opt. Lett.*, **29**, 1581 (2004).

24. Y. Sakakibara, A. G. Rozhin, H. Kataura, Y. Achiba, M. Tokumoto, *Jpn. J. Appl. Phys.*, **44**, 1621 (2005).
25. G. Della Valle, R. Osellame, G. Galzerano, N. Chiodo, G. Cerullo, P. Laporta, O. Svelto, U. Morgner, A. G. Rozhin, V. Scardaci, A. C. Ferrari, *Appl. Phys. Lett.*, **89**, 231115 (2006).
26. V. Scardaci, A. G. Rozhin, F. Hennrich, W. I. Milne, A. C. Ferrari, *Phys. E*, **37**, 115 (2007).
27. V. Scardaci, Z. P. Sun, F. Wang, A. G. Rozhin, T. Hasan, F. Hennrich, I. H. White, W. I. Milne, A. C. Ferrari, *Adv. Mater.*, **20**, 4040 (2008).
28. Z. Sun, A. G. Rozhin, F. Wang, V. Scardaci, W. I. Milne, I. H. White, F. Hennrich, A. C. Ferrari, *Appl. Phys. Lett.*, **93**, 061114 (2008).
29. F. Wang, A. G. Rozhin, V. Scardaci, Z. Sun, F. Hennrich, I. H. White, W. I. Milne, A. C. Ferrari, *Nat. Nano*, **3**, 738 (2008).
30. T. Hasan, Z. Sun, F. Wang, F. Bonaccorso, P. H. Tan, A. G. Rozhin, A. C. Ferrari, *Adv. Mater.*, **21**, 3874 (2009).
31. Z. Sun, A. G. Rozhin, F. Wang, T. Hasan, D. Popa, W. O'Neill, A. C. Ferrari, *Appl. Phys. Lett.*, **95**, 253102 (2009).
32. Z. Sun, T. Hasan, F. Wang, A. Rozhin, I. White, A. Ferrari, *Nano Res.*, **3**, 404 (2010).
33. S. J. Beecher, R. R. Thomson, N. D. Psaila, Z. Sun, T. Hasan, A. G. Rozhin, A. C. Ferrari, A. K. Kar, *Appl. Phys. Lett.*, **97**, 111114 (2010)
34. T. Hasan, V. Scardaci, P. H. Tan, F. Bonaccorso, A. G. Rozhin, Z. Sun, A. C. Ferrari, in O. Hayden, K. Nielsch, eds., *Molecular- and Nano-Tubes*, U.S.: Springer, 2011, 279.
35. C. F. Bohren, D. R. Huffman, *Absorption and Scattering of Light by Small Particles*, New York: Wiley-Interscience, 1998.
36. V. C. Moore, M. S. Strano, E. H. Haroz, R. H. Hauge, R. E. Smalley, *Nano Lett.*, **3**, 1379 (2003).
37. V. Perebeinos, J. Tersoff, P. Avouris, *Phys. Rev. Lett.*, **94**, 027402 (2005).
38. M. S. Arnold, A. A. Green, J. F. Hulvat, S. I. Stupp, M. C. Hersam, *Nat. Nanotechnol.*, **1**, 60 (2006).
39. F. Bonaccorso, T. Hasan, P. H. Tan, C. Sciascia, G. Privitera, G. Di Marco, P. G. Gucciardi, A. C. Ferrari, *J. Phys. Chem. C*, **114** (2010).
40. T. J. McDonald, J. L. Blackburn, W. K. Metzger, G. Rumbles, M. J. J. Heben, *Phys. Chem. C*, **111**, 17894 (2007).
41. H. Qian, C. Georgi, N. Anderson, A. A. Green, M. C. Hersam, L. Novotny, A. Hartschuh, *Nano Lett.*, **8**, 1363 (2008).

42. J. Lefebvre, P. Finnie, *J. Phys. Chem. C*, **113**, 7536 (2009).
43. T. Kato, R. Hatakeyama, *J. Am. Chem. Soc.*, **130**, 8101 (2008).
44. H. Hirori, K. Matsuda, Y. Kanemitsu, *Phys. Rev. B*, **78**, 113409 (2008).
45. F. M. Chen, W. J. Zhang, M. L. Jia, L. Wei, X. F. Fan, J. -L. Kuo, Y. Chen, M. B. Chan-Park, A. D. Xia, L. J. Li, *J. Phys. Chem. C*, **113**, 14946 (2009).
46. F. M. Chen, J. Ye, M. Y. Teo, Y. Zhao, L. P. Tan, Y. Chen, M. B. Chan-Park, L. J. Li, *J. Phys. Chem. C*, **113**, 20061 (2009).
47. R. S. Swathi, K. L. Sebastiana, *J. Chem. Phys.*, **132**, 104502 (2010).
48. J.-H. Han, G. L. C. Paulus, R. Maruyama, D. A. Heller, W.-J. Kim, P. W. Barone, C. Y. Lee, J. H. Choi, M.-H. Ham, C. Song, C. Fantini, M. S. Strano, *Nat. Mater.*, **9**, 833 (2010).
49. L. Luer, J. Crochet, T. Hertel, G. Cerullo, G. Lanzani, *ACS Nano*, **4**, 4265 (2010).
50. T. Koyama, Y. Miyata, Y. Asada, H. Shinohara, H. Kataura, A. Nakamura, *J. Phys. Chem. Lett.*, **1**, 3243 (2010).
51. T. Koyama, K. Asaka, N. Hikosaka, H. Kishida, Y. Saito, A. Nakamura, *J. Phys. Chem. Lett.*, **2**, 127 (2011).
52. T. Koyama, K. Asaka, N. Hikosaka, H. Kishida, Y. Saito, A. Nakamura, *J. Lumin.*, **131**, 494 (2011).
53. X. Dang, H. Yi, Ham, M.-H., J. Qi, D. S. Yun, R. Ladewski, M. S. Strano, P. T. Hammond, A. M. Belcher, *Nat Nano*, **6**, 377 (2011).
54. T. Ignatova, H. Najafov, A. Ryasnyanskiy, I. Biaggio, M. Zheng, S. V. Rotkin, *ACS Nano*, **5**, 6052 (2011).
55. T. Koyama, Y. Asada, N. Hikosaka, Y. Miyata, H. Shinohara, A. Nakamura, *ACS Nano*, **5**, 5881 (2011).
56. T. Förster, *Discuss. Faraday Soc.*, **27**, 7 (1959).
57. M. G. W. Alexander, M. Nido, W. W. Riihle, K. Koehler, *Phys. Rev. B*, **41**, 12295 (1990).
58. S. R. Adams, A. T. Haroontunian, Y. J. Buechler, S. S. Taylor, R. Y. Tsien, *Nature*, **349**, 694 (1991).
59. C. R. Kagan, C. B. Murray, M. Nirmal, M. G. Bawendi, *Phys. Rev. Lett.*, **76**, 1517 (1996).
60. K. Becker, J. Lupton, J. Mueller, A. L. Rogach, D. V. Talapin, H. Weller, J. Feldmann, *Nat. Mater.*, **5**, 777 (2006).
61. V. Biju, T. Itoh, Y. Baba, M. Ishikawa, *J. Phys. Chem. B*, **110**, 26068 (2006).

62. A. Hagen, M. Steiner, M. B. Raschke, C. Lienau, T. Hertel, H. Qian, A. J. Meixner, A. Hartschuh, *Phys. Rev. Lett.*, **95**, 197401 (2005).
63. H. Hirori, K. Matsuda, Y. Miyauchi, S. Maruyama, Y. Kanemitsu, *Phys. Rev. Lett.*, **97**, 257401 (2006).
64. C. D. Spataru, S. Ismail-Beigi, L. X. Benedict, S. G. Louie, *Phys. Rev. Lett.*, **95**, 247402 (2005).
65. S. M. Bachilo, L. Balzano, J. E. Herrera, F. Pompeo, D. E. Resasco, R. B. Weisman, *J. Am. Chem. Soc.*, **125**, 11186 (2003).
66. S. Reich, M. Dworzak, A. Hoffmann, C. Thomsen, M. S. Strano, *Phys. Rev. B*, **71**, 033402 (2005).
67. C. Manzoni, A. Gambetta, E. Menna, M. Meneghetti, G. Lanzani, G. Cerullo, *Phys. Rev. Lett.*, **94**, 207401 (2005).
68. D. A. Heller, E. S. Jeng, T. K. Yeung, B. M. Martinez, A. E. Moll, J. B. Gastala, M. S. Strano, *Science*, **311**, 508 (2006).
69. Y. Ohno, S. Iwasaki, Y. Murakami, S. Kishimoto, S. Maruyama, T. Mizutani, *Phys. Rev. B*, **73**, 235427 (2006).
70. S. Giordani, S. D. Bergin, V. Nicolosi, S. Lebedkin, M. M. Kappes, W. J. Blau, J. N. Coleman, *J. Phys. Chem. B*, **110**, 15708 (2006).
71. Y. Miyauchi, R. Saito, K. Sato, Y. Ohno, S. Iwasaki, T. Mizutani, J. Jiang, S. Maruyama, *Chem. Phys. Lett.*, **442**, 394 (2007).
72. O. Kiowski, S. Lebedkin, F. Hennrich, S. Malik, H. Rosner, K. Arnold, C. Surgers, M. M. Kappes, *Phys. Rev. B*, **75**, 075421 (2007).
73. T. Hasan, V. Scardaci, P. H. Tan, A. G. Rozhin, W. I. Milne, A. C. Ferrari, *J. Phys. Chem. C*, **111**, 12594 (2007).
74. T. Hasan, P. H. Tan, F. Bonaccorso, A. Rozhin, V. Scardaci, W. Milne, A. C. Ferrari, *J. Phys. Chem. C*, **112**, 20227 (2008).
75. S. Reich, C. Thomsen, J. Robertson, *Phys. Rev. Lett.*, **95**, 077402 (2005).
76. T. Okazaki, T. Saito, K. Matsuura, S. Ohshima, M. Yumura, Y. Oyama, R. Saito, S. Iijima, *Chem. Phys. Lett.*, **420**, 286 (2006).
77. Z. T. Luo, L. D. Pfeifferle, G. L. Haller, F. Papadimitrakopoulos, *J. Am. Chem. Soc.*, **128**, 15511 (2006).
78. C. Fantini, A. Jorio, A. P. Santos, V. S. T. Peressinotto, M. A. Pimenta, *Chem. Phys. Lett.*, **439**, 138 (2007).
79. A. Jorio, C. Fantini, M. A. Pimenta, D. A. Heller, M. S. Strano, M. S. Dresselhaus, Y. Oyama, J. Jiang, R. Saito, *Appl. Phys. Lett.*, **88**, 023109 (2006).
80. Y. C. Chen, N. R. Raravikar, L. S. Schadler, P. M. Ajayan, Y. P. Zhao, T. M. Lu, G. C. Wang, X. C. Zhang, *Appl. Phys. Lett.*, **81**(6), 975 (2002).

81. S. Tatsuura, M. Furuki, Y. Sato, I. Iwasa, M. Tian, H. Mitsu, *Adv. Mater.*, **15**, 534 (2003).
82. A. G. Rozhin, Y. Sakakibara, H. Kataura, S. Matsuzaki, K. Ishida, Y. Achiba, M. Tokumoto, *Chem. Phys. Lett.*, **405**, 288 (2005).
83. G. N. Ostojic, S. Zaric, J. Kono, M. S. Strano, V. C. Moore, R. H. Hauge, R. E. Smalley, *Phys. Rev. Lett.*, **92**, 117402 (2004).
84. J. Kono, G. N. Ostojic, S. Zaric, M. S. Strano, V. C. Moore, J. Shaver, R. H. Hauge, R. E. Smalley, *Appl. Phys. A*, **78**, 1093 (2004).